Nanoscale

Phonon transport in nano-system of Si and SiGe films with Ge nanodots and approach to ultralow thermal conductivity

Journal:	*Nanoscale*
Manuscript ID	NR-ART-11-2020-008499.R1
Article Type:	Paper
Date Submitted by the Author:	19-Jan-2021

Complete List of Authors:	Taniguchi, Tatsuhiko; Osaka University Graduate School of Engineering Science School of Engineering Science Terada, Tsukasa; Osaka University Graduate School of Engineering Science School of Engineering Science Komatsubara, Yuki; Osaka University Graduate School of Engineering Science School of Engineering Science Ishibe, Takafumi; Osaka University, Konoike, Kento; Osaka University Graduate School of Engineering Science School of Engineering Science Sanada, Atsushi; Osaka University Graduate School of Engineering Science School of Engineering Science Naruse, Nobuyasu; Shiga University of Medical Science Mera, Yutaka; Shiga University of Medical Science Nakamura, Yoshiaki; Osaka Univ, Grad Sch Engn Sci

SCHOLARONE™
Manuscripts

ARTICLE

Phonon transport in nano-system of Si and SiGe films with Ge nanodots and approach to ultralow thermal conductivity

Received 00th January 20xx,
Accepted 00th January 20xx

DOI: 10.1039/x0xx00000x

Tatsuhiko Taniguchi,[a] Tsukasa Terada,[a] Yuki Komatsubara,[a] Takafumi Ishibe,[a] Kento Konoike,[a] Atsushi Sanada,[a] Nobuyasu Naruse,[b] Yutaka Mera[b] and Yoshiaki Nakamura[a*]

Phonon transport in nano-system has been studied using well-designed nanostructured materials to observe and control the interesting phonon behaviors like ballistic phonon transport. Recently, we observed drastic thermal conductivity reduction in the films containing well-controlled nanodots. Here, we investigate whether this comes from the interference effect in ballistic phonon transport by comparing the thermal properties of the Si or $Si_{0.75}Ge_{0.25}$ films containing Ge nanodots. The experimentally-obtained thermal resistance of the nanodot layer shows peculiar nanodot size dependence in the Si films and constant value in the SiGe films. From the phonon simulation results, interestingly, it was clearly found that in the nanostructured Si film, phonon travels in a non-diffusive way (ballistic phonon transport). On the other hand, in the nanostructured SiGe film, although simple diffusive phonon transport occurs, extremely-low thermal conductivity (~0.81 $Wm^{-1}K^{-1}$) close to that of amorphous $Si_{0.7}Ge_{0.3}$ (~0.7 $Wm^{-1}K^{-1}$) is achieved due to the combination of the alloy phonon scattering and Ge nanodot scattering.

Introduction

Thermal management has been increasingly demanded due to various heat issues; e.g. a vast amount of waste heat, heat generation in miniaturized electronic devices, etc. In the context of managing heat conduction, it is required to comprehensively understand phonon transport characteristics, like behaviors as ballistic phonon transport. To this aim, a lot of researchers have suggested unique nanostructures tailoring phonon transport in light of experiments and theories.[1-19] Coherent phonon effect was observed at room temperature in the superlattices (SLs) with several nm periodicity.[10,18] In the two-dimensional Si phononic crystals with the nanohole periodicity of ~500 nm, the ballistic phonon particle-like transport was detected.[15] On the other hand, the materials containing nanocrystals have been paid attention to for thermal conductivity reduction in the thermoelectric field.[20-32] In such materials, recent theoretical studies reported the interesting phonon wave properties indicating that a nanodot (ND) can work as a resonator in analogy with photonic crystals.[16,19] However, the actual nanostructures include unwanted and undefined structural features, such as interface defect, impurity, strain, etc., making it difficult to classify contribution of each scattering process to phonon transport and especially to observe interesting phonon wave effect.

We have developed the formation technique of well-controlled nanostructures in the films, such as epitaxial NDs with several nm to tends of nm in size.[12,13,17,26,28-30,33-37] Our connected Si NDs exhibited the extremely-low thermal conductivity, κ (~0.78 $Wm^{-1}K^{-1}$) [12] compared with other crystal Si materials. Thanks to the well-controlled nanostructured interfaces, it was revealed that this ultralow κ value was brought by confinement of phonon propagation close to Cahill-Pohl limit.[17] In recent years, we observed the dependence of thermal resistance (TR) on the ND size in Si films containing epitaxial Ge NDs (Ge ND/Si films) (Fig. 1(a)), which is similar to the characteristics of Rayleigh-Mie scatterings in light propagation (Fig. 1(b)).[13] It is intriguing if this comes from wave-like characteristic of phonon. However, it remains unclear whether it is possible to observe the non-diffusive coherent scattering in such nanostructured materials.

In this study, we investigate the existence of the interference effect of the ballistic phonon transport in the films containing well-controlled Ge NDs by comparing Ge ND/Si films with SiGe films containing Ge NDs (Ge ND/SiGe films) because comparing these two nano-systems with/without strong alloy phonon scattering (Figs. 1(c) and (b)) makes it easy to separate ballistic or diffusive transport. The TR in a ND layer, R_{ND}, in the Ge ND/Si films shows the peculiar ND size dependence, whereas the R_{ND} of the Ge ND/SiGe films is almost constant. From finite difference method simulations in diffusive phonon transport and coherent transport, and ND size dependence of the ND cross section, it is concluded that in the Ge ND/Si films, phonon travels in non-diffusive (ballistic) way, while in the Ge ND/SiGe films, diffusive phonon scattering mainly contributes to the heat

[a.] Graduate School of Engineering Science, Osaka University, 1-3 Machikaneyama-cho, Toyonaka, Osaka 560-8531, Japan.
[b.] Department of Fundamental Bioscience, Shiga University of Medical Science, Otsu, Shiga 520-2192, Japan.

†Electronic Supplementary Information (ESI) available: the spatial distribution of NDs, the effect of the ultrathin Si oxide layer on the thermal resistance, assessment of interference effect, simulation of heat conduction in diffusive phonon transport, and simulation in coherent phonon transport. See DOI: 10.1039/x0xx00000x

conduction. Furthermore, due to the ND interface scattering and alloy phonon scattering, the Ge ND/$Si_{0.75}Ge_{0.25}$ films exhibit an ultralow κ value (~0.81 $Wm^{-1}K^{-1}$) which is in the lowest class among reported SiGe-based single-crystal materials including SLs and Stranski-Krastanov (SK) ND SLs. This phonon transport control gives a large impact on the thermal conductivity reduction research in the thermoelectric field.

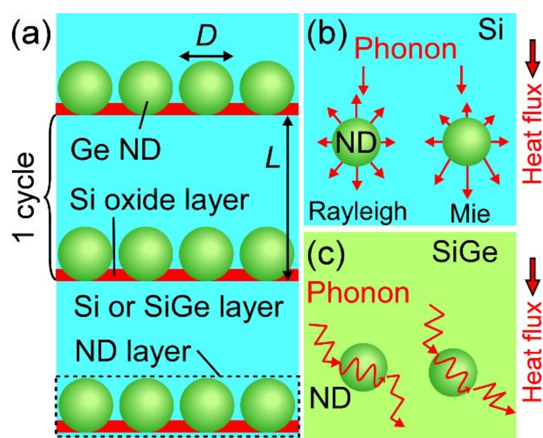

Figure 1 (a) Conceptual illustration of the epitaxial Si or SiGe thin films containing Ge NDs. (b, c) The phonon scattering illustration near the Ge ND in (b) the Si layer and (c) the SiGe layer.

Experimental and computation details

The Ge ND/$Si_{0.75}Ge_{0.25}$ films and the Ge ND/Si films were epitaxially grown on Si(001) substrates (electrical resistivity: ≥1000 Ωcm) using the ultrathin Si oxide film technique in an ultrahigh molecular beam epitaxy chamber equipped with Knudsen cells for Si and Ge at a base pressure of ~1×10^{-8} Pa. The Si substrates were cleaned by a standard wet chemical process using a mixture of sulphuric acid and diluted HF solution. Then, the substrates were introduced into the chamber and degassed at 550°C for ~5h. After 50-nm-Si buffer layers were formed at 500°C to obtain clean Si(001)-(2×1) reconstructed surfaces, the ultrathin Si oxide layers were formed by slightly oxidizing the Si surfaces at 500°C for 10 min under an oxygen pressure of 2×10^{-4} Pa. To fabricate the Ge ND/$Si_{0.75}Ge_{0.25}$ films, the following three process was repeated eight times: (1) Epitaxial Ge NDs (size: 3-25 nm) were formed on the ultrathin Si oxide layers by depositing Ge at 500°C, where nanowindows are formed in the ultrathin Si oxide layers and then the Ge NDs are directly connected with the Si surface through the nanowindows leading to the epitaxial growth. (2) $Si_{0.75}Ge_{0.25}$ layers (12-58 nm) were formed on the Ge NDs by Si and Ge codeposition at ~400°C at the deposition rate of Si and Ge to ~3:1. (3) The ultrathin Si oxide layers were formed by oxidizing the $Si_{0.75}Ge_{0.25}$ layers at 450°C for 10 min under an oxygen pressure of 2×10^{-4} Pa. In the case of the Ge ND/Si films, the Si layers were formed instead of the $Si_{0.75}Ge_{0.25}$ layers in the process (2), and the ultrathin Si oxide layers were formed by oxidizing the Si layers instead of the $Si_{0.75}Ge_{0.25}$ layers in the process (3). According to the previous study,[37] a few monolayer (ML) Ge can diffuse into Si oxide layers. Therefore, the ultrathin Si oxide layers are ~1 ML $Si_{1-z}Ge_zO_y$ layers with a few ML Ge (referred to as "$SiGeO_y$") in Ge ND/$Si_{0.75}Ge_{0.25}$ films and ~1 ML SiO_2 layers with a few ML Ge (referred to as "SiO_2-Ge") in the Ge ND/Si films. In this way, the Ge ND/SiGe films and the Ge ND/Si films were fabricated by stacking one cycle structure eight times, where the one cycle structure is composed of $Si_{0.75}Ge_{0.25}$ (or Si) layers with layer thicknesses, L, and Ge NDs with the size D on the Si oxide layers with a few ML thickness (Fig. 1(a)). The epitaxial stacked films are referred to as the Ge ND (D)/$Si_{0.75}Ge_{0.25}$ (L) film or Ge ND (D)/Si (L) film. To investigate the effect of the Si oxide layers, we also fabricated the ND free samples that is the Ge ND (0 nm)/$Si_{0.75}Ge_{0.25}$ films and the Ge ND (0 nm)/Si film. In these samples, $Si_{0.75}Ge_{0.25}$ NDs and Si NDs were grown instead of Ge NDs in the process (1), respectively. The Ge ND (0 nm)/$Si_{0.75}Ge_{0.25}$ film has one cycle structure, not stacked one. The details of the Ge ND/Si films were also described elsewhere.[13,26,29,30,35]

In-situ reflection high-energy electron diffraction (RHEED) observations were performed with 20 keV electron beam incident in the <110>$_{Si}$ direction. High resolution scanning transmission electron microscopy observations were performed with 200 keV electron beam incident in the <110>$_{Si}$ direction. The κ values along the cross-plane direction at room temperature were measured by 2ω method,[12,38,39] where we preliminarily deposited Au transducer films on the samples for detection of thermoreflectance signal. In the κ analysis, the interfacial thermal resistance between the Au films and the sample surfaces was removed using the reported value of 1.9×10^{-8} m^2KW^{-1}.[13] In-situ scanning tunneling microscopy (STM) observations were carried out to determine D and ND coverage at room temperature using sharp W tip.[40] The ND coverage corresponds to the ND cross sectional ratio, θ in the view of perpendicular direction to the film.

To estimate the R_{ND} values in the films containing Ge NDs in the diffusive phonon transport, we simulated the temperature distribution of the one cycle structure using three dimensional heat conduction equation, which details are described in the ESI†. To calculate the transmitted and reflected energy in the coherent phonon transport, elastic wave propagation in three dimensional media was simulated on the linearized elasticity theory and a stress-stiffness tensor formulation, which details are described in the ESI†.

Results and discussion

Structural analyses of films containing Ge NDs formed by ultrathin Si oxide film technique

Figure 2(a) shows the RHEED pattern of the $Si_{0.75}Ge_{0.25}$ layer in the 8th cycle structure of the Ge ND (~8 nm)/$Si_{0.75}Ge_{0.25}$ (~22 nm) film. This spotty pattern indicated that the $Si_{0.75}Ge_{0.25}$ layer was epitaxially grown with rough surface. Figure 2(b) shows the

This journal is © The Royal Society of Chemistry 20xx

low-magnification cross-sectional annular dark field transmission electron microscopy (ADF-TEM) image of the Ge ND (~8 nm)/$Si_{0.75}Ge_{0.25}$ (~22 nm) film. Although the roughness of the $Si_{0.75}Ge_{0.25}$ layers gradually increased with the stacking number of one cycle structure, which is consistent with the RHEED result, because of the rough morphology of the Ge NDs, the stacked structure was well formed; the Ge NDs with quasi-uniform size (bright spots) were periodically separated by the $Si_{0.75}Ge_{0.25}$ layers. Figure 2(c) shows the enlarged image of the region near the Ge NDs (the region marked by the dotted square in Fig. 2(b)). The Ge NDs (marked by the dashed lines) had the hemispherical structures and there was dark line of ultrathin Si oxide layer below the Ge NDs. There were almost no defects at the interfaces of NDs/ Si oxide / $Si_{0.75}Ge_{0.25}$ layer. The ultrathin Si oxide layer was composed of ~1 ML $Si_{1-z}Ge_zO_y$ formed by oxidizing $Si_{0.75}Ge_{0.25}$ layer and a few ML Ge ($SiGeO_y$), where Ge atoms diffused into the Si oxide layer during the growth.[37] Thus, the epitaxial $Si_{0.75}Ge_{0.25}$ films containing uniformly-sized Ge NDs/Si oxide layers with almost no defects were formed. On the other hand, in the case of the Ge ND/Si films, the structure analyses were reported elsewhere, and it was confirmed that the Si films contained well-controlled Ge NDs/ultrathin Si oxide layer with almost no defects like the Ge ND/$Si_{0.75}Ge_{0.25}$ films.[13,26,29,30,35] The ultrathin Si oxide layer in the Ge ND/Si film was composed of ~1 ML SiO_2 formed by oxidizing Si layer and the diffused Ge (SiO_2-Ge).[37] Note that it was reported that the NDs formed by the ultrathin oxide films were randomly distributed with almost constant separation on the underlying layer[13,26,28,29,33] and in this paper, we confirmed this distribution of Ge NDs on the Si or SiGe layers (see ESI†).

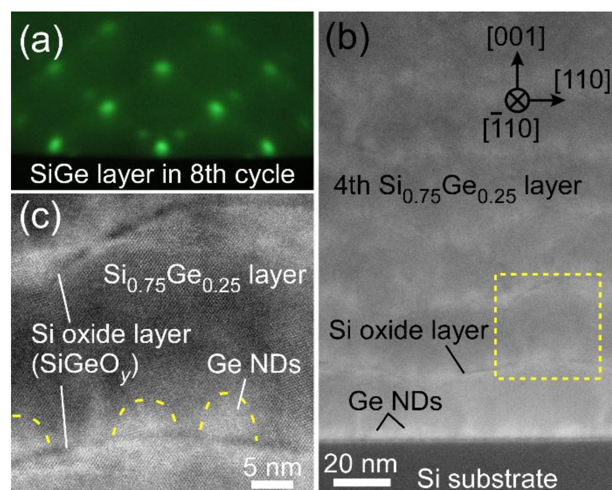

Figure 3 (a) RHEED pattern of the $Si_{0.75}Ge_{0.25}$ layer in the 8th cycle structure of the Ge ND (~8 nm)/$Si_{0.75}Ge_{0.25}$ (~22 nm) film. (b, c) Cross-sectional ADF-TEM images of the Ge ND (~8 nm)/$Si_{0.75}Ge_{0.25}$ (~22 nm) film: (b) low and high (c) magnifications. The image in (c) is corresponding to the region marked by the dotted square in (b).

Thermal conductivities of epitaxial films containing Ge NDs

Figure 3(a) shows the κ values of the Ge ND/$Si_{0.75}Ge_{0.25}$ films and the Ge ND/Si films as a function of L with other reported values.[13,41-43] In the whole L range, our Ge ND/$Si_{0.75}Ge_{0.25}$ films exhibited lower κ values than those of the Ge/Si SLs,[41,42] the SK Ge NDs/SiGe SLs,[43] and our Ge ND/Si films.[13] The Ge ND (~8 nm)/$Si_{0.75}Ge_{0.25}$ (~12 nm) film exhibited the ultralow κ value of ~0.81 $Wm^{-1}K^{-1}$ which is close to amorphous $Si_{0.7}Ge_{0.3}$ (~0.7 $Wm^{-1}K^{-1}$),[44] and is in the lowest class in the ever-reported SiGe-based single-crystal materials. This highlights that the Ge ND/$Si_{0.75}Ge_{0.25}$ films formed using the ultrathin Si oxide film technique can be a good thermoelectric material in terms of low κ. It should be noted that the dependencies of κ on the ND size and on the L in the Ge ND/$Si_{0.75}Ge_{0.25}$ films differed from those in the Ge ND/Si films. The κ values of the Ge ND/$Si_{0.75}Ge_{0.25}$ films did not depend on the ND sizes, whereas the Ge ND/Si films showed the increasing κ tendency with the ND size decrease. The Ge ND/$Si_{0.75}Ge_{0.25}$ films displayed the weak L dependence of κ unlike the Ge ND/Si films with the strong L dependence. Therefore, the present size dependence difference reveals that the contribution of the Ge NDs to phonon transport in the Ge ND/$Si_{0.75}Ge_{0.25}$ films is substantially smaller than in the Ge ND/Si films. Note that it is difficult to simply compare with reported size dependence of two-dimensional materials[45] because of the

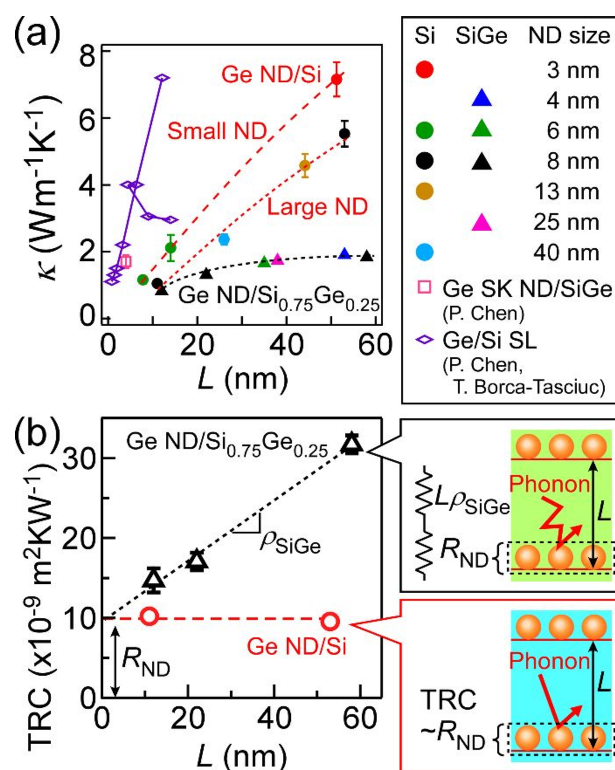

Figure 2 The L dependence of (a) κ and (b) TRC. In (a), the red dashed and the red dotted lines are the eye-guides for the Ge ND/Si films with the small and the large Ge ND sizes, respectively. The black dotted line is the eye-guide for the Ge ND/$Si_{0.75}Ge_{0.25}$ films. In (b), the black dotted line for the Ge ND (8 nm)/$Si_{0.75}Ge_{0.25}$ film is the line-fitted curve with eqn (1) and the red dashed line for the Ge ND (8 nm)/Si film shows no dependence of TRC on the L. R_{ND} values for the Ge ND/Si films are roughly consistent with those of our previous study.[13] In the right side of (b), the schematics of one cycle structures, and the thermal circuit model of the Ge ND/SiGe films: TRC=$L\rho_{SiGe}$+R_{ND}.

different measurement direction: normal thermal transport for our films (stacking structures of ND layers), and transverse and longitudinal thermal transport for the reported two-dimensional materials.[45]

To clarify the contribution of the Ge NDs to phonon transport, the thermal resistance per one cycle structure (TRC) was experimentally acquired by dividing the total TR of the films by the stacked number of 8. Figure 3(b) shows L dependencies of TRC in the Ge ND (~8 nm)/$Si_{0.75}Ge_{0.25}$ films and the Ge ND (~8 nm)/Si films. The TRC values of the Ge ND/Si films were constant when increasing L, revealing that phonon scattering in Si layers is negligible in the heat conduction in the Ge ND/Si films. Namely heat conduction is dominated by phonon transport in a ND layer. Then, when TR created by phonon transport in a ND layer is described as R_{ND}, R_{ND} is equal to the TRC in the Ge ND/Si film case. On the other hand, in the case of the Ge ND/$Si_{0.75}Ge_{0.25}$ films, the TRC values monotonically increased with L, which is presumably due to the alloy phonon scattering in SiGe layers. Therefore, we assumed the thermal circuit model, as shown in the right side of Fig. 3(b). Therein, the TRC is modeled by

$$\mathrm{TRC}=L\rho_{SiGe}+R_{ND} \quad (1),$$

where ρ_{SiGe} is a thermal resistivity of the SiGe layer and R_{ND} is a TR in the Ge ND layer. By fitting the TRC with eqn (1), the ρ_{SiGe} and R_{ND} were acquired to be ~0.38 ± 0.03 mKW^{-1} and (8.1±1.9) $\times10^{-9}$ m^2KW^{-1}, respectively. The ρ_{SiGe} value almost agreed with the thermal resistivity of the epitaxial $Si_{0.75}Ge_{0.25}$ films on the ultrathin Si oxide films on Si (~0.45 ± 0.01 mKW^{-1}) (see ESI†), validating this circuit analysis model. Thus, R_{ND} values, which are the prevention of phonon transport by the Ge NDs, were well extracted from the total TRC by this analysis.

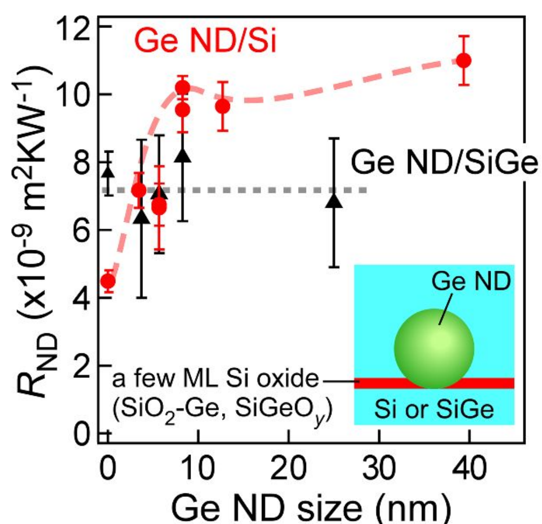

Figure 4 The Ge ND size dependence of R_{ND} of the Ge ND/Si films (the red circles) and the Ge ND/$Si_{0.75}Ge_{0.25}$ films (the black triangles). The dashed and dotted curves are the eye-guides.

In the case of Ge ND/$Si_{0.75}Ge_{0.25}$ films, the diffusive phonon transport was presumably dominant in the whole structures because the thermal circuit model was applicable. However, there is a possibility that the R_{ND} itself, the prevention of phonon transport by the Ge NDs, might originate from the feature of the coherent phonon in the nano-system. To investigate the origin of TR created by phonon transport in a ND layer, the R_{ND} values in the Ge ND/$Si_{0.75}Ge_{0.25}$ films with various ND sizes were estimated from eqn (1) using ρ_{SiGe} of ~0.38 mKW^{-1} as mentioned above, while those in the case of the Ge NDs/Si films were obtained by TRC. The R_{ND} values are plotted as a function of the Ge ND size in Fig. 4. R_{ND} values at ND size of 0 were measured for the film structures of $Si_{0.75}Ge_{0.25}$ or Si / Si oxide (ND-free structure), exhibiting thermal resistance caused by the ultrathin Si oxide film without NDs (see ESI†). The R_{ND} for the Ge ND/$Si_{0.75}Ge_{0.25}$ film case is almost constant in the whole ND size range, where the uncertainty is relatively large due to the estimation with eqn (1). R_{ND} values for the Ge ND/Si films are roughly consistent with those of our previous study.[13] It should be noted that R_{ND} value for the Ge ND/Si film case shows the peculiar tendency; R_{ND} increases when the ND sizes increases up to ~15 nm, and R_{ND} is saturated in the ND size of >~15 nm. At first, we simulated the R_{ND} values using three dimensional heat conduction equation in the diffusive phonon transport (see ESI†). As mentioned above, the actual one cycle structure is composed of the Si or $Si_{0.75}Ge_{0.25}$ layers and the Ge NDs on a few ML thick Si oxide (SiO_2-Ge or $SiGeO_y$) as shown in the inset of Fig. 4. The thermal properties (the thermal resistances and interfacial thermal resistances) of the Si oxide layers (SiO_2-Ge or $SiGeO_y$) are unknown because they have SiO_2 or $Si_{1-z}Ge_zO_y$ with just ~1 ML thickness and could include a few Ge ML.[37] Therefore, in this simulation, we used the experimental R_{ND} value at ND size of 0 as the thermal properties of these ultrathin Si oxide layers in the inset of Fig. 5(a). We also used the values of the interfacial thermal resistance of the Si/Ge (3.1×10^{-9} m^2KW^{-1}),[46] and the κ values of Si (156 $Wm^{-1}K^{-1}$),[47] $Si_{0.75}Ge_{0.25}$ (7.7 $Wm^{-1}K^{-1}$)[48] and Ge (60 $Wm^{-1}K^{-1}$),[47] and the interfacial thermal resistance of the $Si_{0.75}Ge_{0.25}$/Ge was estimated to be 1.66×10^{-9} m^2KW^{-1} from that of the Si/Ge by assuming that the interfacial thermal resistance is linear to the atomic mass ratio.[46,49] As shown in Fig. 5(a), the simulated R_{ND}s were constant in the whole Ge ND size range, except for R_{ND} at ND size of ~40 nm for the Ge ND/Si film case. In the Ge ND/$Si_{0.75}Ge_{0.25}$ film case, the simulation results reproduced the experimental result (Fig. 4), indicating that diffusive phonon transport is dominant in this nano-system presumably due to the strong alloy phonon scattering. On the other hand, in the Ge ND/Si film case, it should be noted that the diffusive phonon transport cannot explain the peculiar tendency of the experimental R_{ND}, implying the possibility of ballistic phonon transport in the nano-system. In the coherent phonon transport in this nanostructure, it is expected that scattering probability (related to thermal resistance) becomes larger when the Ge ND size becomes larger than the wavelength of the phonon carrying heat dominantly in analogy with Rayleigh-Mie scatterings of light.[50]

In the Ge ND/Si film cases with ballistic phonon transport, we simulated coherent phonon transport by linear elastodynamic simulation (see ESI†). A typical simulated

This journal is © The Royal Society of Chemistry 20xx

schematic and a simulated wave distribution of the coherent phonon transport are shown in Figs. 5(b) and (c). A Gaussian-enveloped coherent vibration pulse with the root-mean-square speed in Bose distributions at 300K was applied at each node on the input plane above the Ge ND in Fig. 5(b) independently to the static system, and the scattered wave transport was simulated. Then, as shown in Fig. 5(d), the total reflected energy ratio was calculated using the equation of $1-T_D/T_0$, where T_0 and T_D are the transmitted wave energies without the Ge ND and the Si oxide layer and with Ge ND size of D nm, respectively. In the ND size less than 15 nm, the tendency of the reflected energy ratio roughly agrees with that of ND-size dependence of the experimental R_{ND} in the Ge ND/Si film case (Fig. 4). Figure 5(d) also reveals that there seemed to be an offset value (~0.8) related to high reflected energy ratio at ND size of 0. These results indicate that phonon can travel coherently in one cycle structure with NDs sandwiched by the ultrathin Si oxide layer although most phonons transmit through the ultrathin Si oxide layer non-coherently. In a typical simulated image in Fig. 5(c), a long wavelength standing phonon wave exists inside a ND. This indicates that the ND can work as a resonator like phononic crystals. However, it was difficult to find the clear resonance feature in the ND-size dependence of reflected energy ratio in this ND size range. Even if some phonons with certain wavelengths are resonated, the heat conduction caused by various phonons does not always exhibit the resonance feature. Furthermore, transmission spectrum reveals that the transmitted wave spectrum is limited within the frequency range less than THz, implying that the ND-size dependence of the experimental R_{ND} in the Ge ND/Si film case is due to low-frequency phonons as shown in the Fig. S5(c) in the ESI†. This is also consistent with phonon wave-packet dynamics,[51] which supports reliability of our simulation.

As mentioned above, there was no clear resonance feature of the ND coming from coherent interference in the heat conduction. Therefore, we discuss the interference effect by comparing the ballistic phonon transports with/without interference (see ESI†). Particle-like phonon model traveling straight among the interfaces is virtually considered as the ballistic phonon transport without interference. In this virtual phonon transport model, the scattering probability of heat flow by ND is proportional to the θ value because NDs are target for the particles traveling straight. We estimated the θ values in the view of perpendicular direction to the film, which is corresponding to the ND coverage (see experimental method and ESI†), as shown in Fig. 5(d). The dependence of the θ value on the ND size also roughly agrees with the R_{ND} in the Ge ND/Si films (Fig. 4) in the smaller ND size range (<~15 nm), indicating that the predicted ND size dependence of R_{ND} in the virtual ballistic phonon transport without interference has a similar tendency of that in coherent transport (ballistic transport with interference). This indicates that it is difficult to identify the interference effect such as resonance feature in the experimental ND-size dependence of R_{ND} in the Ge ND/Si film case. However, the present experiment revealed that phonon travels in non-diffusive way in Ge ND/Si system with the ND size less than ~15 nm unlike Ge ND/SiGe system. This finding comes from the fabrication of well-controlled ND structures into the two largely-different systems in terms of phono transport: Si and SiGe layers.

On the other hand, the lack of the dependence of R_{ND} values in the Ge ND/$Si_{0.75}Ge_{0.25}$ films is because large contribution of diffusive alloy phonon scattering in the $Si_{0.75}Ge_{0.25}$ layers hides that of resonance effect in the Ge ND, even if the Ge NDs work as resonators for phonon. However, in terms of aiming at the smallest thermal conductivity in single crystals, it is a remarkable fact that the combination of the strong alloy phonon scattering and the scattering by ultrasmall NDs actually bring the ultralow κ in epitaxial crystals: ~0.81 $Wm^{-1}K^{-1}$ in the Ge ND/$Si_{0.75}Ge_{0.25}$ film close to the amorphous value (~0.7 $Wm^{-1}K^{-1}$ for $Si_{0.7}Ge_{0.3}$).[44] This gives a large impact on the thermal conductivity reduction research in the thermoelectric field.

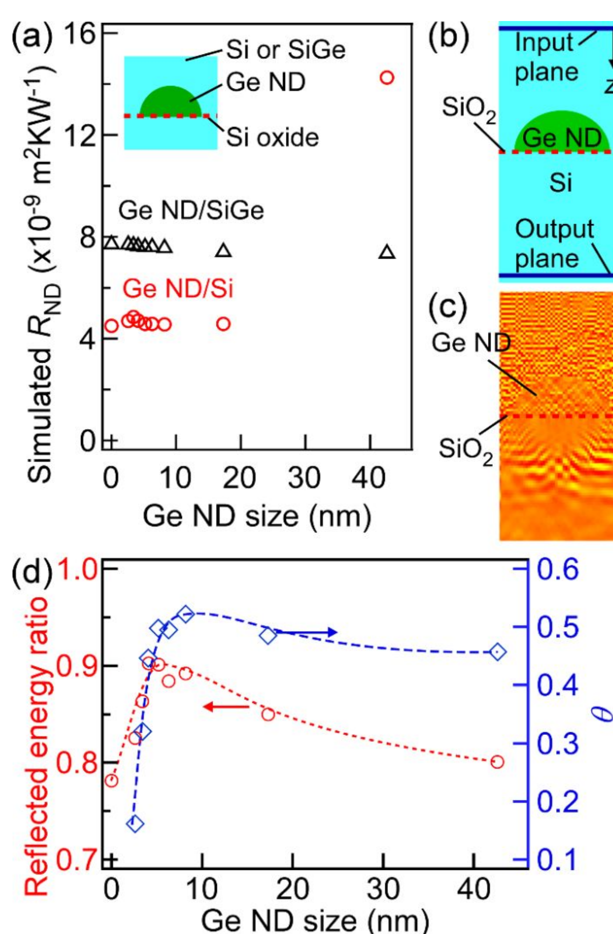

Figure 5 (a) The Ge ND size dependence of the simulated R_{ND} by heat conduction in diffusive phonon transport. The inset in (a) is a simulated schematic. (b) The simulated schematic and (c) a typical simulated wave distribution image (*zz*-component of the stress tensor) at time of ~60 fs after inputting coherent vibration pulse in the coherent phonon transport. (d) The Ge ND size dependence of the reflected energy ratio obtained from simulation of coherent phonon transport (left axis) and the Ge ND coverage (right axis). The dotted and dashed lines are the eye-guides of the reflected energy ratio and θ, respectively.

This journal is © The Royal Society of Chemistry 20xx

Conclusions

This study investigated the phonon transport in the well-controlled Ge ND system by comparing the thermal properties of the Ge ND/Si films with those of the Ge ND/SiGe films. The R_{ND} displayed a peculiar ND size dependence in the Ge ND/Si films, while in the Ge ND/SiGe films, the R_{ND} shows the constant value because the diffusive alloy phonon scattering in the SiGe layers was dominant. The heat conduction simulation in diffusive phonon transport precisely reproduced the experimental data in the Ge ND/SiGe films. On the other hand, in the Ge ND/Si films, from the simulation of coherent phonon transport and the cross-sectional ND ratio result, it was found that the peculiar ND size dependence of R_{ND} comes from the ballistic phonon transport. In addition, the Ge ND/$Si_{0.75}Ge_{0.25}$ films exhibited ultralow κ value (~0.81 $Wm^{-1}K^{-1}$) close to the amorphous value (~0.7 $Wm^{-1}K^{-1}$ for $Si_{0.7}Ge_{0.3}$), which obtained value is in the lowest class in reported SiGe-based single crystal materials including SLs and SK ND SLs. This gives a large impact on the thermal conductivity reduction research in the thermoelectric field.

Author Contributions

T. Taniguchi fabricated the samples, measured thermal characteristics and performed structural analysis. T. Terada measured the surface morphology. T. Taniguchi and T. I. analyzed the data. Y. N. is a principal investigator of this work. T. Taniguchi, Y. K., T. I., A. S. and Y. N. discussed the phonon transport physics. T. Taniguchi, Y. K., T. I., and Y. N. wrote the manuscript. K. K. and A. S. simulated thermal characteristics. N. N. and Y. M. carried out the TEM experiments.

Conflicts of interest

There are no conflicts to declare.

Acknowledgements

This work was supported by a Grant-in-Aid for Scientific Research A (19H00853), Exploratory Research (19K22110), and JSPS Research fellow (18J20160) from JSPS KAKENHI, Japan. This work was also supported in part by the JST CREST Grant No. JPMJCR1524. A part of this work was conducted at the Hokkaido University, supported by "Nanotechnology Platform Program" of the Ministry of Education, Culture, Sports, Science and Technology (MEXT), Japan, Grant Number JPMXP09A20HK0036.

Notes and references

1 G. Chen, Phys. Rev. Lett. 2001, **86**, 2297.
2 G. Xie, D. Ding, and G. Zhang, Adv. Phs.: X, 2018, **3**, 1480417.
3 D. G. Cahill, W. K. Ford, K. E. Goodson, G. D. Mahan, A. Majumdar, H. J. Maris, R. Merlin, and S. R. Phillpot, J. Appl. Phys., 2003, **93**, 793.
4 B. Yang, and G. Chen, Phys. Rev. B, 2003, **67**, 195311.
5 P. G. Murphy, and J. E. Moore, Phys. Rev. B, 2007, **76**, 155313.
6 J. Chen, G. Zhang, and B. Li, J. Chem. Phys., 2011, **135**, 104508.
7 M. N. Luckyanova, J. Garg, K. Esfarjani, A. Jandl, M. T. Bulsara, A. J. Schmidt, A. J. Minnich, S. Chen, M. S. Dresselhaus, Z. Ren, E. A. Fitzgerald, and G. Chen, Science, 2012, **338**, 936.
8 A. M. Marconnet, M. Asheghi, and K. E. Goodson, J. Heat Transfer, 2013, **135**, 061601.
9 Y. Wang, H. Huang, and X. Ruan, Phys. Rev. B, 2014, **90**, 165406.
10 J. Ravichandran, A. K. Yadav, R Cheaito, P. B. Rossen, A. Soukiassian, S. J. Suresha, J. C. Duda, B. M. Foley, C.-H. Lee, Y. Zhu, A. W. Lichtenberger, J. E. Moore, D. A. Muller, D. G. Schlom, P. E. Hopkins, A. Majumdar, R. Ramech, and M. A. Zurbuchen, Nat. Mater., 2014, **13**, 168.
11 S. Alaie, D. F. Goettler, M. Su, Z. C. Leseman, C. M. Reinke, and I. El-Kady, Nat. Commum., 2015, **6**, 7228.
12 Y. Nakamura, M. Isogawa, T. Ueda, S. Yamasaka, H. Matsui, J. Kikkawa, S. Ikeuchi, T. Oyake, T. Hori, J. Shiomi, and A. Sakai, Nano Energy, 2015, **12**, 845.
13 S. Yamasaka, Y. Nakamura, T. Ueda, S. Takeuchi, and A. Sakai, Sci. Rep., 2015, **5**, 14490.
14 J. Lee, W. Lee, G. Wehmeyer, S. Dhue, D. L. Olynick, S. Cabrini, C. Dames, J. J. Urban, and P. Yang, Nat. Commun., 2017, **8**, 14054.
15 R. Anufriev, A. Ramiere, J. Marie, and M. Nomura, Nat. Commun., 2017, **8**, 15505.
16 L. Feng, T. Shiga, H. Han, S. Ju, Y. A. Kosevich, and J. Shiomi, Phys. Rev. B, 2017, **96**, 220301.
17 T. Oyake, L. Feng, T. Shiga, M. Isogawa, Y. Nakamura, and J. Shiomi, Phys. Rev. Lett., 2018, **120**, 045901.
18 R. Hu, S. Iwamoto, L. Feng, S. Ju, S. Hu, M. Ohnishi, N. Nagai, K. Hirakawa, and J. Shiomi, Phys. Rev. X, 2020, **10**, 021050.
19 S. Hu, L. Feng, C. Shao, I. A. Strelnikov, Y. A. Kosevich, and J. Shiomi, Phys. Rev. B, 2020, **102**, 024301.
20 G. Joshi, H. Lee, Y. Lan, X. Wang, G. Zhu, D. Wang, R. W. Gould, D. C. Cuff, M. Y. Tang, M. S. Dresselhaus, G. Chen, Z. Ren, Nano Lett., 2008, **8**, 4670.
21 X. W. Wang, H. Lee, Y. C. Lan, G. H. Zhu, G. Joshi, D. Z. Wang, J. Yang, A. J. Muto, M. Y. Tang, J. Klatsky, S. Song, M. S. Dresselhaus, G. Chen, and Z. F. Ren, Appl. Phys. Lett., 2008, **93**, 183121.
22 S. K. Bux, R. G. Blair, P. K. Gogna, H. Lee, G. Chen, M. S. Dresselhaus, R. B. Kaner, and J.-P. Fleurial, Adv. Funct. Mater., 2009, **19**, 2445.
23 B. Yu, M. Zebarjadi, H. Wang, K. Lukas, H. Wang, D. Wang, C. Opeil, M. Dresselhaus, G. Chen, and Z. Ren, Nano Lett., 2012, **12**, 2077.
24 D. Narducci, G. Cerofolini, M. Ferri, F. Suriano, F. Mancarella, L. Belsito, S. Solmi, and A. Roncaglia, J. Mater. Sci., 2013, **48**, 2779.
25 S. Bathula, M. Jayasimhadri, B. Gahtori, N. K. Singh, K. Tyagi, A. K. Srivastava, and A. Dhar, Nanoscale, 2015, **7**, 12474.
26 S. Yamasaka, K. Watanabe, S. Sakane, S. Takeuchi, A. Sakai, K. Sawano, and Y. Nakamura, Sci. Rep., 2016, **6**, 22838.
27 T. Ishibe, A. Tomoda, K. Watanabe, Y. Kamakura, N. Mori, N. Naruse, Y. Mera, Y. Yamashita, and Y. Nakamura, ACS Appl. Mater. Interfaces, 2018, **10**, 37709.
28 Y. Nakamura, Sci. Tech. Adv. Mater., 2018, **19**, 31.
29 S. Sakane, T. Ishibe, T. Taniguchi, N. Naruse, Y. Mera, T. Fujita, M. M. Alam, K. Sawano, N. Mori, and Y. Nakamura, Mater. Today Energy, 2019, **13**, 56.
30 S. Sakane, T. Ishibe, T. Hinakawa, N. Naruse, Y. Mera, M. M. Alam, K. Sawano, and Y. Nakamura, Appl. Phys. Lett., 2019, **115**, 182104.

This journal is © The Royal Society of Chemistry 20xx

Please do not adjust margins

31 N. Liu, S. E. Rezaei, W. A. Jensen, S. Song, Z. Ren, K. Esfarjani, M. Zebarjadi, and J. A. Floro, Adv. Funct. Mater., 2019, **29**, 1903157.
32 T. Taniguchi, T. Ishibe, N. Naruse, M. Yutaka, Md. M. Alam, K. Sawano, and Y. Nakamura, ACS Appl. Matter. Interfaces, 2020, **12**, 25428.
33 Y. Nakamura, A. Masada, and M. Ichikawa, Appl. Phys. Let., 2007, **91**, 013109.
34 Y. Nakamura, A. Murayama, R. Watanabe, T. Iyoda, M. Ichikawa, Nanotechnology, 2010, **21**, 095305.
35 S. Yamasaka, Y. Nakamura, T. Ueda, S. Takeuchi, Y. Yamamoto, S. Arai, T. Tanji, N. Tanaka, and A. Sakai, J. Electron. Mater., 2015, **44**, 2015.
36 T. Ishibe, Y. Maeda, T. Terada, N. Naruse, Y. Mera, E. Kobayashi, and Y. Nakamura, Sci. Tech. Adv. Mater., 2020, **21**, 195.
37 N. Tanaka, S.-P. Cho, A. A. Shklyaev, J. Yamasaki, E. Okunishi, and M. Ichikawa, Appl. Surf. Sci., 2008, **254**, 7569.
38 K. Mitarai, R. Okuhata, J. Chikada, T. Kaneko, Y. Uematsu, Y. Komatsubara, T. Ishibe, and Y. Nakamura, J. Appl. Phys., 2020, **128**, 015102.
39 Y. Uematsu, T. Terada, K. Sato, T. Ishibe, and Y. Nakamura, Appl. Phys. Express, 2020, **13**, 055503.
40 Y. Nakamura, Y. Mera, and K. Maeda, Rev. Sci. Instrum., 1999, **70**, 3373.
41 T. Borca-Tasciuc, W. Liu, J. Liu, T. Zeng, D. W. Song, C. D. Moore, G. Chen. K. L. Wang, and M. S. Goorsky, Superlattices Microstruct., 2000, **28**, 199.
42 P. Chen, N. A. Katcho, J. P. Feser, W. Li, M. Glaser, O. G. Schmidt, D. G. Cahill, N. Ming, and A. Rastelli, Phys. Rev. Lett., 2013, **111**, 115901.
43 P. Chen. J. J. Zhang, J. P. Feser, O. Moutanabbir, S. Cecchi, G. Isella, T. Gemming, S. Baunack, G. Chen, O. G. Schmidt, and A. Rastelli, J. Appl. Phys., 2014, **115**, 044312.
44 J. L. Feldman, M. D. Kluge, P. B. Allen, and F. Wooten, Phys. Rev. B, 1993, **48**, 12589.
45 Z. Zhang, Y. Ouyang, Y. Cheng, J. Chen, N. Li, and G. Zhang, Phys. Rep. 2020, **860**, 1.
46 E. S. Landry, and A. J. H. McGaughey, Phys. Rev. B, 2009 **80**, 165304.
47 C. J. Glassbrenner, and G. A. Slack, Phys. Rev., 1964, **134**, A1058.
48 J. P. Dismukes, L. Ekstrom, E. F. Steigmeier, I. Kudman, and D. S. Beers, J. Appl. Phys., 1964, **35**, 2899.
49 J. A. Katerberg, C. L. Reynolds, Jr., and A. C. Anderson, Phys. Rev. B, 1977, **16**, 673.
50 W. Kim, and A. Majumdar, J. Appl. Phys., 2006, **99**, 084306.
51 P. K. Schelling, S. R. Phillpot, and P. Keblinski, Appl. Phys. Lett., 2002, **80**, 2484.